Heliyon 9 (2023) e13685

Contents lists available at ScienceDirect

Heliyon

journal homepage: www.cell.com/heliyon

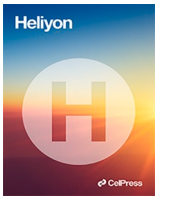

Research article

In silico studies, X-ray diffraction analysis and biological investigation of fluorinated pyrrolylated-chalcones in zebrafish epilepsy models

Muhammad Syafiq Akmal Mohd Fahmi [a,1], Puspanjali Swain [b,1], Amirah Hani Ramli [c], Wan Norhamidah Wan Ibrahim [c,d], Nur Atikah Saleh Hodin [d,e], Noraini Abu Bakar [d], Yee Seng Tan [f], Siti Munirah Mohd Faudzi [a,c,*], Cheol-Hee Kim [b,**]

[a] *Department of Chemistry, Faculty of Science, Universiti Putra Malaysia, 43400 UPM, Serdang, Selangor, Malaysia*
[b] *Department of Biology, Chungnam National University, 99 Daehak-ro, Yuseong-gu, Daejeon 34134, South Korea*
[c] *Natural Medicines and Product Research Laboratory, Institute of Bioscience, Universiti Putra Malaysia, Serdang, 43400, Selangor, Malaysia*
[d] *Department of Biology, Faculty of Science, Universiti Putra Malaysia, 43400 UPM, Serdang, Selangor, Malaysia*
[e] *Centre of Foundation Studies for Agricultural Science, Universiti Putra Malaysia, Serdang, 43400, Selangor, Malaysia*
[f] *Research Centre for Crystalline Materials, School of Medical and Life Sciences, Sunway University, 47500 Bandar Sunway, Selangor Darul Ehsan, Malaysia*

ARTICLE INFO

Keywords:
Chalcones
Antiepileptic drugs (AEDs)
Zebrafish

ABSTRACT

Epilepsy is the third most common known brain disease worldwide. Several antiepileptic drugs (AEDs) are available to improve seizure control. However, the associated side effects limit their practical use and highlight the ongoing search for safer and effective AEDs. Eighteen newly designed fluorine-containing pyrrolylated chalcones were extensively studied in silico, synthesized, structurally analyzed by X-ray diffraction (XRD), and biologically and toxicologically tested as potential new AEDs in zebrafish epilepsy in vivo models. The results predicted that 3-(3,5-difluorophenyl)-1-(1*H*-pyrrol-2-yl)prop-2-en-1-one (compound **8**) had a good drug-like profile with binding affinity to γ-aminobutyric acid receptor type-A ($GABA_A$, −8.0 kcal/mol). This predicted active compound **8** was effective in reducing convulsive behaviour in pentylenetetrazol (PTZ)-induced larvae and hyperactive movements in *zc4h2* knockout (KO) zebrafish, experimentally. Moreover, no cardiotoxic effect of compound **8** was observed in zebrafish. Overall, pyrrolylated chalcones could serve as alternative AEDs and warrant further in-depth pharmacological studies to uncover their mechanism of action.

1. Introduction

Epilepsy is the fourth most common neurological disorder worldwide after migraine, stroke, and Alzheimer's disease [1], with most

* Corresponding author. Department of Chemistry, Faculty of Science, Universiti Putra Malaysia, 43400 UPM, Serdang, Selangor, Malaysia.
** Corresponding author.
E-mail addresses: sitimunirah@upm.edu.my (S.M. Mohd Faudzi), zebrakim@cnu.ac.kr (C.-H. Kim).
[1] These authors contributed equally.

https://doi.org/10.1016/j.heliyon.2023.e13685
Received 25 September 2022; Received in revised form 7 February 2023; Accepted 8 February 2023
Available online 11 February 2023

newly discovered cases occurring in children and adults. Approximately 50 million people suffer from epilepsy globally, and nearly 80% of epilepsies occur in developing countries, including Malaysia. Alarmingly, the lifetime prevalence of epilepsy in Malaysia is 7.8

Abbreviation

AEDs	antiepileptic drugs
XRD	X-ray diffraction
$GABA_A$	γ-aminobutyric acid receptor type-A
PTZ	pentylenetetrazol
VPA	sodium valproate
KO	knockout
ADMET	absorption, distribution, metabolism, excretion, and toxicity
PAINS	pan-assay interference compounds
WT	Wild Type
hpf	hour post-fertilization
dpf	day post-fertilization
LC_{50}	Lethal Concentration at 50%
STC	spontaneous tail coiling
EW	Egg water
SEM	standard error mean
CADD	Computer-aided drug design
ZC4H2	C4H2-type of zinc finger

per 1000 persons according to recent studies [2]. Epilepsy can be characterized by the electrical activity of the brain as a transient occurrence of signs and/or symptoms due to abnormal excessive or synchronous neuronal activity in the brain [3]. It is mainly caused by epileptogenesis, which can lead to dysfunction of central nervous system (CNS) neurons, particularly glutamatergic and ϒ -aminobutyric acid (GABA)-ergic neurons. During epileptogenesis, genetic mutations in the brain can induced the expression of ion channels and regulatory proteins, resulting in an imbalance in excitation and inhibition of cation discharges [4,5]. If left untreated, epilepsy can lead to severe impaired consciousness, movement disorders, and sensory disturbances (visual, auditory, and gustatory), as well as death [6].

Antiepileptic drug (AED) therapy is the common treatment for most patients with epilepsy. Several newer AEDs have been tested in comparative trials and have shown equivalent efficacy and tolerability to older AEDs as first-line therapy, including lamotrigine, oxcarbazepine, levetiracetam, topiramate, zonisamide, and lacosamide [7]. However, some AEDs can negatively affect mood, behaviour, or cognition. For example, levetiracetam has been associated with worsening quality of life in children, lamotrigine is more likely to be a mood-altering AED, and ezogabine has been withdrawn from the market due to potential retinal toxicity. In addition, the use of common AEDs, including benzodiazepines (BZD), sodium valproate (VPA), and carbamazepine (CBZ), may contribute to side effects such as severe dependence and high risk when used during pregnancy [8]. This underscores the urgent need to continue searching for newer, effective, and safe medications (AEDs) for the treatment of epilepsy.

Subsequently, continuous efforts have been made to develop new AED alternatives with improved efficacy and safety profiles, including chalcones as a new class of AEDs. Chalcones, a compound consisting of α, β-unsaturated ketones, is an important class of drugs that has been the subject of numerous preclinical and clinical investigations due to their efficacy in treating diseases. Various aromatic substituents offer the possibility of enhancing the therapeutic value of the chalcone backbone, including antitumor, anti-inflammatory, and antimicrobial effects with lower toxicity [9,10]. Previously, 2- and 3-fluoropyrrolylated chalcones (Fig. 1) with significant antiseizure activity were discovered from our library in zebrafish model [11]. In addition, previous literatures have shown structure-activity relationships (SARs) suggesting that the fluorophenyl moiety is essential for significant anticonvulsant/antiepileptic activities [12–18].

Following these discoveries, a series of eighteen fluorinated pyrrolylated chalcones (**1**–**18**, Fig. 2) were designed, studied in silico in detail (including physicochemical prediction and molecular docking), chemically synthesized, and biologically evaluated (toxicologically and behaviourally) as potential new AEDs in the pentylenetetrazol (PTZ)-induced seizure and *zc4h2* knockout (KO) zebrafish in vivo model. Fluorine was chosen as a substituent because it has been shown to improve several pharmacokinetic and physicochemical properties, including metabolic stability, which in turn increases the solubility of the analogues. In addition, fluorine can also affect the electronic modulation, steric parameters, and lipophilicity of the drug, thus increasing the potency of the compound [19]. Meanwhile, the zebrafish (*Danio rerio*) was selected as an in vivo model for validation of antiepileptic effects due to its rapid life cycle, high spawning number, transparent zebrafish embryos and larvae with a large repertoire of neurological behaviours. The zebrafish, one of the most unique vertebrate models, perfectly meets these requirements and has become an experimental model for numerous CNS studies over the past two decades because it resembles other vertebrates in terms of general brain organization [20].

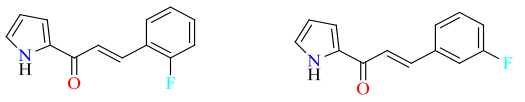

Fig. 1. Structure of (a) 2- and (b) 3-fluoropyrrolylated chalcones [11].

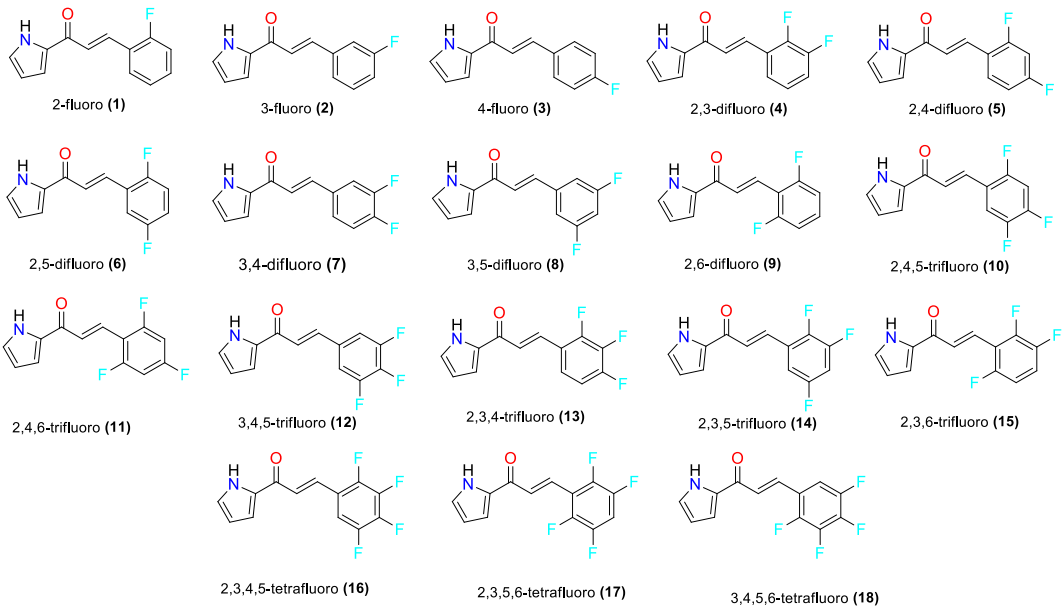

Fig. 2. Structures of the fluorine-containing pyrrolylated chalcones (**1**–**18**).

2. Materials and methods

2.1. In silico

2.1.1. Physicochemical and ADMET filtration

Physiochemical properties are one of the filters to assess the drug-like nature of compounds. All 2D chemical structures of the designed molecules (**1**–**18**) were drawn using ChemDraw Ultra 12.0 to create the Simplified Molecular Input Line Entry System (SMILES). Subsequently, the SMILES were converted to Symyx Spatial Data File (SDF) format using OpenBabel 3.1.1. As recommended by the FAF-Drugs4 Bank Formatter (https://mobyle.rpbs.univ-paris-diderot.fr/cgi-bin/portal.py?form=FAF-%20Drugs4#forms::FAF-Drugs4) before being imported as an input file into the FAF-Drugs4 Web Server (http://mobyle.rpbs.univ-paris-diderot.fr/cgi-bin/portal.py?form=FAF-Drugs3#forms::FAF-Drugs4). Meanwhile, the same SDF file of the designed compounds was imported into ChemAGG web server (https://admet.scbdd.com/ChemAGG/index/) to predict possible aggregators. The results of aggregator identification were displayed in scores: aggregator (1) and non-aggregator (0). Finally, ADMET profiles and PAINS identification could be generated by inserting the existing SMILES into SwissADME (https://admet.scbdd.com/ChemAGG/index/) and the ADMETlab 2.0 web server (https://admet.scbdd.com/calcpre/index/).

2.1.2. Molecular docking

Molecular docking was performed to investigate the possible interactions and binding affinity between the newly designed fluorine-containing pyrrolylated chalcones (**1**–**18**) and the standard drugs (BEN500 and VPA) at the $GABA_A$ receptor to predict their antiepileptic potential. The crystal structure of a human γ-aminobutyric acid receptor, $GABA_A$R-beta3 homopentamer (PDB ID: 4COF), was downloaded from the RCSB Protein Data Bank (https://www.rcsb.org/). The protein was prepared using AutoDock Tools version 1.5.6 by adding polar hydrogen, assigned charges to the $GABA_A$ receptor, and saved as. pdbqt. All ligands, water, small molecules and residues were removed using Discovery Studio Visualizer v19.1.0.18,287 and saved in. pdb format. Docking input files were generated from a search grid box with the following parameters: Center x: 9.099, Center y: 22.493, Center z: 116.764 with dimensions Size x: 40, Size y: 40, and Size z: 40, with spacing, was set to 1 and saved in dock. txt format.

All newly designed ligands (compound **1**–**18**) and the standard drugs of BEN500 and VPA were optimized with Avogadro software version 1.2.0 using the General Amber Force Field (GAFF) and saved in a. pdb file. Subsequently, all hydrogen atoms were added and defined as ligands using AutoDock tool version 1.5.6 and saved in the pdbqt file. Docking programming was performed using

automatic docking software (AutoDock Vina). The final poses with the best docking score generated by Vina were selected and visually analyzed using Discovery Studio Visualizer v19.1.0.18,287 to determine the binding affinities and interactions formed between the enzyme and ligands in 2D and 3D representation (Figures S1-S19 in Supplementary Material).

2.2. Chemistry

2.2.1. Synthesis

The synthesis was adapted based on [21], where the predicted active antiepileptic chalcone, compound **8**, was synthesized by a one-pot Claisen-Schmidt condensation reaction, purified and structurally characterized single crystal X-ray diffraction technique. Synthetically, 2 mmol of 2-acetylpyrrole (0.22 g) and 3,5-difluorobenzaldehyde (218 μL) were dissolved in 5 mL of 95% ethanol and the mixture was stirred for 5 min, followed by the dropwise addition of 1 mL of NaOH (6 M). The reaction mixture was then stirred overnight at room temperature. Once the reaction was complete, crushed ice was added to quench the reaction, followed by the addition of dilute HCl to neutralize the reaction mixture before another extraction with ethyl acetate (3 × 10 mL). The organic layer was collected, dried with anhydrous $MgSO_4$, and evaporated under reduced pressure. The crude products were purified by column chromatography (hexane: ethyl acetate) and recrystallized with methanol to give pure compound **8**.

The resulting purified **8** was a yellow solid (69.72%); mp 151–152 °C; IR (UATR) 3243 (NH), 1649 (C═O), 1581 (C═C), 1301 (*C*–F) cm^{-1}; ^{1}H NMR (500 MHz, acetone-d_6) δ: 6.34 (m, 1H, Py-H), 7.09 (tt, J = 2.3 and 9.1 Hz, 1H, Ar–H), 7.26 (m, 1H, Py-H), 7.39 (m, 1H, Py-H), 7.50 (br. d, J = 2.1 Hz, 1H, Ar–H), 7.52 (br. d, J = 2.1 Hz, 1H, Ar–H), 7.67 (d, J_{trans} = 15.7 Hz, 1H, CH═CH), 7.79 (d, J_{trans} = 15.7 Hz, 1H, CH═CH), 11.10 (br. s, 1H, NH); ^{13}C NMR (125 MHz, acetone-d_6) δ: 104.5, 110.3, 110.9, 111.1, 117.0, 125.5, 126.1, 133.3, 138.1, 139.3, 162.3, 164.3, 177.3; ^{19}F NMR (470 MHz, acetone-d_6) δ: 111.1; HRMS (ESI): *m/z* calculated for $C_{13}H_9F_2NO$–H^-: 232.0580 [M − H]$^-$; found: 232.0569. All the spectroscopic spectrum could be view in Supplementary Material (Figures S20–26).

2.2.2. X-ray crystallography of (E)-3-(3,5-difluorophenyl)-1-(1h-pyrrol-2-yl)prop-2-en-1-one

Crystals of the most predicted active compound **8** were grown by slow evaporation of ethanol. Intensity data of the 'plate-like' colorless crystals of compound **8** were measured at 100 K using a Rigaku/Oxford Diffraction XtaLAB Synergy diffractometer (Dualflex, AtlasS2) with CuKα radiation (λ = 1.54184 Å). Data processing and Gaussian absorption corrections were performed using CrysAlis Pro [22], while the structure was solved by dual space direct methods using ShelXT [23]. Refinement was performed using the full-matrix least squares method (on F^2) with anisotropic shift parameters for all non-hydrogen atoms [24]. The crystallographic analysis also included the use of the programs ORTEP-3 for Windows [25], PLATON [26], and DIAMOND [27]. The crystallographic data of compound **8** have been deposited at the Cambridge Crystallographic Data Center (CCDC) and are available for reference (Deposit Number: 2,203,560). More detailed experiments on XRD analysis are included in the Supplementary Material (Section S3.1).

2.3. In vivo studies

2.3.1. Generation of zc4h2 KO zebrafish

The zebrafish *zc4h2* KO was generated using TALEN (transcription activator-like effector nuclease), as previously reported [28]. A TALEN vector targeting the second exon of *zc4h2* was developed and assembled by ToolGen Inc (http://toolgen.com/). The TALEN vectors were linearized with *Pvu*II and purified by ethanol precipitation. Subsequently, mRNAs encoding the left and right TALENs were synthesized using the mMESSAGE mMACHINE T7 Transcription Kit (Ambion catalog number AM1344) and purified by phenol/chloroform precipitation. Following that, single-cell fertilized embryos were mincroinjected with TALEN mRNAs, which were then grown to 4 months of adulthood.

A stable mutant line of *zc4h2* was identified, DNA genotyped and purified by the phenol/chloroform method, in which DNA was first extracted from single larvae or fin-cut adult tissues and lysed with genomic DNA isolation buffer (10 mM Tris, 50 mM EDTA, 200 mM NaCl, 0.5% SDS, and 0.5 mg/mL proteinase K) for 12 h at 55 °C. Direct PCR and sequencing was then performed using the following primer pairs and PCR conditions: *zc4h2* exon2 forward primer, 5′-GACCGAGTTGAAGTCTGG-3'; *zc4h2* exon2 reverse primer, 5′-CACGTTAATATCCGCATGAATG-3'. The 130 bp PCR products were purified by gel extraction and analyzed by the T7 endonuclease I assay (NEB catalog number M0302).

2.3.2. Zebrafish husbandry

All PTZ-induced WT experiments were approved by the Institutional Animal Care and Use Committee (IACUC) of the Animal Ethics Committee of Universiti Putra Malaysia (IACUC/AUP-R079). Meanwhile, experiments using *zc4h2* KO zebrafish were performed in accordance with the approved Institutional Animal Care and Use Committee (IACUC) guidelines and regulations of Chungnam National College (Approval number: CNU 00191), and the desired KO zebrafish were obtained from the Zebrafish Center for Disease Modeling (ZCDM; Daejeon, Republic of Korea).

Adult zebrafish (WT and *zc4h2* KO strains), all older than 6 months were maintained in 2-L aquaria at 25–27 °C on a 10:14 h dark-light cycle. Fish were maintained at a ratio of 2 males: 3 females in a single tank to provide a stress-free environment. The WT and KO fish were each fed brine shrimp (Artemia, Super Artemia (M) Sdn Bhd, Shah Alam, Selangor, Malaysia), and alternated between brine shrimp (Artemia, INVE aquaculture Inc, Salt Lake City, UT, USA) and commercial flake food (Gemma Micro 75 zf, skretting France, Le Pont de Pierre, France), 3 to 4 times per day. The aquarium water system was maintained by a constant circulation pump.

2.3.3. Toxicity profiling of embryo zebrafish

A series of toxicity assessments [spontaneous tail coiling (STC), hatching rate, mortality, and lethal concentration at 50% (LC_{50})] were initially conducted based on the preliminary study (Anuar, 2019; unpublished results) to ensure safe, maximum, non-toxic concentrations of compound **8**. In this study, six concentrations of compound **8** (0, 4.29, 8.58, 12.86, 17.15, and 21.44 μM) prepared by serial dilution of the 1 mM stock solution (0.012 g of compound **8** dissolved in 5 mL DMSO), were exposed to healthy wild-type (WT) zebrafish embryos at the 5-h post-fertilization (hpf), including the control. Experiments were performed in triplicate, with 10 embryos placed in each well of the 12-well plates ($n = 30$). At 24 hpf, embryos were habituated for 5 min, and assessment was performed by manually counting the number of STC for 1 min (a complete coil is indicated by the movement of the larvae's trunk side to side [29]). Subsequently, the percentage of hatched embryos at 72 hpf was determined by calculating the percentage of hatched embryos out of all incubated embryos in the well. Mortality was also recorded daily throughout the exposure period to determine the LC_{50} endpoint at 72 hpf. All endpoints were observed using a standard dissecting microscope (SZX-12, Olympus, Tokyo, Japan).

2.3.4. Antiepileptic behavioural effect of compound 8 on PTZ-induced epilepsy larvae of

2.3.4.1. Zebrafish. To better understand the antiepileptic effects of compound **8**, behavioural assessments were performed. Larvae were exposed to three different compounds: PTZ (to induce epilepsy), VPA (positive control), and compound **8**; with concentrations selected based on previous literature [30]. The stock solution of 1 M PTZ and 100 mM VPA was prepared by dissolving 0.1382 g PTZ and 0.01 g VPA salt in 1 mL distilled water, respectively. In addition, a concentration of 8.58 μM of compound **8** was selected based on the toxicity studies performed. Different exposure regimens were applied in 24 well plates (control/egg water; PTZ only; VPA only; compound **8** only; PTZ + VPA; and PTZ + compound **8**), with each well filled with one larva ($n = 30$). Exposure began with a treatment of 2.5 mM PTZ to 5 dpf larvae that were incubated for 15 min. After PTZ exposure, 100 μM VPA and 8.58 μM compound **8** (VPA only; PTZ + VPA; compound **8** only; and PTZ + compound **8**) were added simultaneously and incubated for 1 h. Treated larvae were then acclimatized for 15 min before a series of behavioural assessments were performed to rule out confounding factors such as anxiety and stress due to the new environment. Behavioural endpoints included basic locomotor responses (total speed, average speed, total distance, average distance, and thigmotaxis) and freezing activity (total number of freezing, average number of freezing, total duration of freezing, and average duration of freezing). All behavioural assays were performed automatically for 15 min under continuous illumination and quantified using Zebrabox behavioural software (ZebraLab, Viewpoint, Life Sciences, Inc., Montreal, Canada). Protocols were optimized according to the manual provided with some modifications based on previous studies [31,32]. A graphical representation of this method can be found in Figure S20 (in Supplementary Material).

2.3.5. Evaluation of antiepileptic and cardiotoxic effect of compound 8 in the zc4h2 KO zebrafish model

The 5 dpf ZARD KO larvae that exhibited abnormal swimming behaviour with loss of the swim bladder and a ventrally curved trunk were collected, and six individuals per well were placed in a 48-well plate containing 300 μl of egg water (EW, 180 μg/mL sea salt (S9883; Sigma-Aldrich, St. Louis, MO) in distilled water). To each well were added 300 μl of 0.1% DMSO, 2.5, 5, 10, 20, 40, and 80 μM of compound **8**. After the 2-h exposure, a single larva was observed on a zebrafish resistance array device and the movements of the jaw were recorded for 1 min. The locomotor movement of each larva were recorded with a Leica DFC450C digital camera (Leica TL5000 Ergo transmitted-light base) and processed using Leica Application Suite (Leica, Wetzlar, Germany). Consequently, the cardiotoxic property of compound **8** was also evaluated by analyzing the heartbeat at 5 dpf. 10 larvae per concentration were placed in a 48-well plate and incubated for 2 h. Heartbeats/min were counted using a Leica DFC450C digital camera (Leica TL5000 Ergo transmitted light base).

2.3.6. Statistical analysis

All obtained results were generated as mean ± standard error mean (SEM) and calculated using GraphPad Prism 9.3.0 (San Diego, CA, USA). Normality test was performed before proceeding with one-way analysis of variance (ANOVA) for the toxicity profile and antiepileptic behavioural effect to obtain p values, followed by Tukey's post hoc test. $P \leq 0.05$ was considered significantly different from the other treatment groups. Meanwhile, Pearson's correlation was used to evaluate the correlation between the total freezing count and locomotion (total speed measured) for the PTZ-induced group treated with compound **8** (PTZ+**8** group).

3. Results and discussions

3.1. In silico

Computer-aided drug design (CADD) is critical in the drug discovery and development process for the cost-effective identification of promising drug candidates [33]. These computational methods, i.e., in silico filtering and molecular docking, are important to support the rational design of new and safe drug candidates, to estimate the binding energy of protein-ligand complexes using scoring functions, and to structurally map the binding position of compounds in the cavities of proteins-of-interest to select the best-scored compounds for subsequent synthesis and validation by biological assays. Therefore, all designed fluorine-containing pyrrolylated chalcones (**1**–**18**; designed based on the previous SARs and commercially available fluorinated benzaldehydes) were subjected to in silico studies prior to molecular docking, including physicochemical, aggregator, pan-assay interference compounds (PAINS), and absorption, distribution, metabolism, excretion, and toxicity (ADMET) predictions to pre-screen the drug-like properties of the

compounds.

3.1.1. Physicochemical and ADMET filtration

The prediction of physiochemical properties is an important parameter for evaluating the characteristic of drug-likeness, for prioritizing candidate drugs from a set of designed molecules, and for screening out chemicals that are likely to pose certain physical or toxicological hazards [34]. Physiochemical properties, including Lipinski's Rule of 5 (RO5), i.e., molecular weight (MW), octanol-water partition coefficient (log P), hydrogen bond donor (HBD) and hydrogen bond acceptor (HBA), as well as total polar surface area (TPSA) and non-rotational bonding (NRB), can be generated with FAFDrug4, as shown in Table 1. RO5 is defined as combined parameters that can be used to identify a potential drug candidate that may have absorption and permeability issues [35,36]. This rule states that a compound must not violate more than one criterion: MW $\leq$ 500, log P $\leq$ 5, HBD $\leq$5 and HBA $\leq$10.

In addition, it is critical to identify common structural motifs that may affect false-positive results [known as pan-assay interference compounds (PAINS)] early in the drug discovery process. This screening is usually performed prior to synthesis to verify that the biological function of a designed compound is as expected [37]. Moreover, it is crucial that all compounds are also screened for their aggregation properties, as the tested compound tends to spontaneously form colloids with the protein, aggregate, interfere, and thus experimentally lead to false-positive results [38]. The result presented in Table 1 confirms that none of the designed fluorinated chalcones (**1**–**18**) violates RO5 and does not exhibit aggregation tendencies (probability is less than 1), therefore, all compounds are referred to as non PAINS-associated molecules.

Moreover, VEBER-based prediction of drug-likeness states that NRB $\leq$10 and TPSA $\leq$140 are prerequisites for pre-selection of orally active drugs. In addition, the prediction of oral bioavailability, as suggested by the EGAN rule, listed the following criteria: (a) good bioavailability for compounds with 0 $\geq$ TPSA $\leq$132 Å^2 and -1 $\geq$ log P $\leq$ 6 [39] and (b) good orally available compounds with -1 $\leq$ log P $\leq$ 5.8, TPSA $\leq$130 Å^2 [40]. Table 2 shows that all compounds (**1**–**18**) are predicted to have good oral bioavailability, which correlates with EGAN and VEBER rules.

Phospholipidosis and carbon fraction sp^3 (Fsp^3) are additional variables that influence the prediction of good drug bioavailability. It is worth noting that the accumulation of phospholipids in the lysosome is a hallmark of drug-induced phospholipidosis (PLD), in which excessive accumulation can impair cell viability. Therefore, it is important to test compounds for their ability to induce PLD early in the drug design process. The results presented in Table 2 show that not all compounds induce PLD, highlighting the predicted high bioavailability of the designed chalcones. On the other hand, Fsp^3, the fraction of sp3-hybridised carbons in a molecule relative to its total carbon content, is used to evaluate the spatial complexity of a molecule and estimate its carbon saturation [41]. A higher Fsp^3 value is predicted for better solubility and increases the clinical success rate of a drug candidate [42]. Unfortunately, low solubility was predicted for all designed compounds **1**–**18** (Fsp^3 = 0).

In silico screening of ADMET properties is also critical in the early stages of drug discovery and development to predict the drug-likeness and viability of therapeutic candidates. ADMET properties allow scientists to learn more about the safety and efficacy aspects of a drug candidate, as ADMET is often used to describe the mechanisms of intestinal wall passage, intercompartmental movement, drug metabolism, excretion and transport, as well as the pharmacokinetic properties of compounds [43]. The predicted ADMET properties of chalconoids (**1**–**18**), including blood-brain barrier (BBB), human intestinal absorption (HIA), inhibition of CYP2C19, inhibition of *P*-glycoprotein (PgP), and binding to plasma proteins (PPB) are summarized in Table 2.

BBB is an important parameter often associated with the CNS-based route of drug administration. It is understandable that drugs targeting the CNS should possessing higher BBB penetration, and in contrast, drugs targeting peripheral organs should have lower BBB penetration to minimise adverse effects on the CNS. BBB penetration can be classified as follows: (a) strong BBB penetration to the CNS >2.0, (b) moderate BBB penetration to the CNS, 0,1 < BBB <2,0, and (c) weak BBB absorption to the CNS <0.1 [44]. Our results (see Table 2) suggest that all fluorinated compounds have moderate BBB penetration, which allowed them to undergo further structural

Table 1
Physiochemical properties, PAINS and aggregation information of compounds **1**–**18**.

Compound	MW (g/mol)	Log P	HBD	HBA	RO5 Violations	PAINS	Aggregator Probability	TPSA (Å)	NRB
1	215.22	3.12	1	2	0	No	0.160	32.86	3
2	215.22	2.91	1	2	0	No	0.080	32.86	3
3	215.22	2.91	1	2	0	No	0.139	32.86	3
4	233.21	3.01	1	3	0	No	0.063	32.86	3
5	233.21	3.01	1	3	0	No	0.132	32.86	3
6	233.21	3.01	1	3	0	No	0.105	32.86	3
7	233.21	3.01	1	3	0	No	0.064	32.86	3
8	233.21	3.01	1	3	0	No	0.063	32.86	3
9	233.21	3.01	1	3	0	No	0.070	32.86	3
10	251.20	3.11	1	4	0	No	0.059	32.86	3
11	251.20	3.11	1	4	0	No	0.060	32.86	3
12	251.20	3.11	1	4	0	No	0.074	32.86	3
13	251.20	3.11	1	4	0	No	0.112	32.86	3
14	251.20	3.11	1	4	0	No	0.047	32.86	3
15	251.20	3.11	1	4	0	No	0.053	32.86	3
16	269.19	3.21	1	5	0	No	0.083	32.86	3
17	269.19	3.21	1	5	0	No	0.048	32.86	3
18	269.19	3.21	1	5	0	No	0.083	32.86	3

Table 2
Drug likeness and ADMET properties of compounds **1**–**18**.

Compound	Oral bioavail-ability (VEBER)	Oral bioavail-ability (EGAN)	Phospho-lipidosis	Fsp^3	BBB	HIA	CYP2C19 inhibition	PgP inhibition	PPB
1	Good	Good	Non inducer	0	0.433	0.006	Inhibitor	Inhibitor	97.32
2	Good	Good	Non inducer	0	0.554	0.007	Inhibitor	Inhibitor	97.61
3	Good	Good	Non inducer	0	0.483	0.006	Inhibitor	Inhibitor	97.41
4	Good	Good	Non inducer	0	0.396	0.005	Inhibitor	Inhibitor	97.98
5	Good	Good	Non inducer	0	0.535	0.005	Inhibitor	Inhibitor	98.24
6	Good	Good	Non inducer	0	0.452	0.005	Inhibitor	Inhibitor	98.36
7	Good	Good	Non inducer	0	0.475	0.005	Inhibitor	Inhibitor	98.33
8	Good	Good	Non inducer	0	0.599	0.006	Inhibitor	Inhibitor	98.35
9	Good	Good	Non inducer	0	0.315	0.004	Inhibitor	Inhibitor	98.01
10	Good	Good	Non inducer	0	0.528	0.005	Inhibitor	Inhibitor	98.25
11	Good	Good	Non inducer	0	0.495	0.005	Inhibitor	Inhibitor	98.43
12	Good	Good	Non inducer	0	0.521	0.005	Inhibitor	Inhibitor	97.87
13	Good	Good	Non inducer	0	0.379	0.005	Inhibitor	Inhibitor	98.41
14	Good	Good	Non inducer	0	0.496	0.005	Inhibitor	Inhibitor	98.19
15	Good	Good	Non inducer	0	0.288	0.004	Inhibitor	Inhibitor	98.46
16	Good	Good	Non inducer	0	0.314	0.004	Inhibitor	Inhibitor	97.94
17	Good	Good	Non inducer	0	0.318	0.004	Inhibitor	Inhibitor	98.49
18	Good	Good	Non inducer	0	0.314	0.004	Inhibitor	Inhibitor	97.94

*Fsp^3 (carbon fraction sp^3), BBB (Blood Brain Barrier), HIA (Human Intestinal Absorption), PgP inhibition (*P*-glycoprotein) and PPB (Plasma Protein Binding).

modifications to be considered as effective molecules for the treatment of CNS disorders. Meanwhile, the poor HIA and bioavailability of drugs after oral administration, often exacerbated by poorly soluble compounds, remains one of the major challenges in drug discovery. In general, an effective drug should have a low HIA value (HIA <30%). Encouragingly, the low HIA values predicted for all compounds **1**–**18** indicate favourable drug-like properties [45]. Moreover, in humans, the drug is metabolised by the CYP2C19 or cytochrome P450 enzyme, so a CYP2C19 inhibitor should increase plasma levels of the drug [46]. Oxcarbazepine and felbamate are examples of CYP inhibitors that have been shown to be effective AEDs in previous studies. Therefore, evaluating the inhibitory properties of CYP2C19 is critical in the search for new AED candidates, and compounds **1** to **18** are all predicted to be CYP2C19 inhibitors, highlighting their AED potential (Table 2).

PgP is a member of the ATP-binding cassette transporters (ABC), which transport various chemicals across cell membranes and are widely distributed in the intestinal epithelium [47]. Recent studies have shown that the endothelial cells of the BBB of epilepsy patients overexpress PgP. Some studies also suggest that several AEDs may be PgP substrates or inhibitors, raising the possibility that PgP plays an important role in drug resistance in patients with refractory epilepsy. Compounds 1 to 18 were predicted to be PgP inhibitors based on Table 2, indicating their potential efficacy as AEDs. On the other hand, PPB is useful for calculating the amount of a drug that is unbound per effective concentration when using drugs that inhibit transporters and metabolising enzymes, which may result in an unpleasant response [48]. PPB could be characterized as (a) strongly bound compounds (PPB >90%) and (b) weakly bound compounds (PPB <90%). All designed chalcones showed strong binding affinity with protein plasma as indicated in Table 2.

Based on the in silico studies, most of the molecules showed good physicochemical properties, non-PAINS, and non-aggregator, with good ADMET profiles, except for the low solubility predicted by reference to Fsp^3 ($Fsp^3 = 0$).

3.1.2. Molecular docking

Molecular docking was performed to gain functional and structural insights into the binding mode of compounds **1**–**18** to the human ϒ-aminobutyric acid receptor, the GABA(A)R-β3 homopentamer (PDB ID: 4COF), and their binding affinity. Several amino acid chains play a crucial role in ensuring efficient binding of the ligand in a crystal structure of a $GABA_A$ receptor. According to Ref. [49], the critical binding sites, termed neurotransmitter pockets, are located between the extracellular domain (ECD) consisting of the β4-strand and its adjacent residues (Asp95- Leu99), as well as part of the β7-β8 loop (Glu155- Tyr159) and the β9- β10 loop (Phe200-Tyr205).

First, a validation study had to be performed to prove that the binding site was acceptable for docking. To this end, the co-

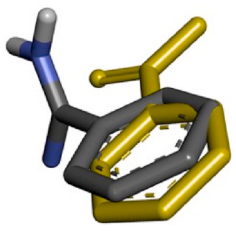

Fig. 3. The validation of co-crystallized and re-docked BEN500.

Table 3
Binding affinity and selected binding interactions of compounds **1**–**18** and VPA with the active site residues of the $GABA_A$ receptor.

Compounds	Binding Affinity (kcal/mol)	Protein-ligand interactions			
		1 Ligand	Receptors	Interactions	Bonding distance (Å)
1	−7.8	-F	Asp43	Halogen (F)	3.34
2	−7.6	*N*–H	Thr176	H bond	2.44
3	−7.7	*N*–H	Asn41	H bond	2.19
		-F	Tyr97	H bond	3.02
		-F	Glu155	Halogen (F)	3.13
		-F	Tyr157	Halogen (F)	3.30
		-F	Ser156	Halogen (F)	3.49
4	−7.7	*N*–H	Asn41	H bond	3.01
		-F	Thr202	H bond	2.87
		-F	Tyr97	H bond	3.66
5	−7.9	-F	Glu155	Halogen (F)	2.90
		2	Glu155	Halogen (F)	2.97
		-F			
		-F	Asp43	Halogen (F)	3.11
6	−7.9	-F	Glu155	Halogen (F)	2.81
		-F	Asp43	Halogen (F)	3.05
		C=O	Arg180	H bond	6.02
7	−7.8	-F	Glu155	Halogen (F)	3.04
		-F	Tyr97	H bond	3.25
		C=O	Thr202	H bond	3.21
8	−8.0	*N*–H	Asn41	H bond	2.24
		-F	Glu155	Halogen (F)	3.43
9	−7.3	-F	Asp43	Halogen (F)	2.89
		-F	Gln64	H bond	3.36
		-F	Thr202	H bond	3.07
		C=O	Thr176	H bond	3.38
10	−7.8	-F	Glu155	Halogen (F)	3.34
		-F	Tyr157	Halogen (F)	3.08
		-F	Tyr157	Halogen (F)	3.47
		-F	Ser156	Halogen (F)	5.92
		C=O	Asn41	H bond	2.38
11	−7.7	-F	Gln64	Halogen (F)	3.53
		-F	Asn41	Halogen (F)	3.45
		N–H	Glu155	H bond	2.43
		N–H	Tyr97	H bond	2.46
12	−7.9	*N*–H	Asn41	H bond	2.76
		-F	Asp43	Halogen (F)	3.03
		-F	Tyr97	H bond	2.82
		-F	Glu155	Halogen (F)	2.84
		-F	Glu155	Halogen (F)	3.09
13	−8.3	-F	Glu155	Halogen (F)	3.37
		-F	Ser156	Halogen (F)	3.37
		-F	Tyr157	Halogen (F)	2.98
		-F	Tyr157	Halogen (F)	2.71
		-F	Gln64	H bond	3.19
		N–H	Asn41	H bond	2.24
14	−8.2	*N*–H	Asn41	H bond	1.95
		-F	Tyr157	Halogen (F)	4.51
		-F	Tyr97	H bond	3.12
		-F	Glu155	Halogen (F)	3.10
		-F	Asp43	Halogen (F)	2.77
15	−6.6	-F	Tyr62	H bond	3.19
16	−8.4	*N*–H	Leu99	H bond	2.71
17	−8.1	-F	Gln64	H bond	3.30
		-F	Thr202	H bond	3.14
		-F	Tyr157	Halogen (F)	3.19
		-F	Glu155	Halogen (F)	3.18
		-F	Tyr97	H bond	3.19
		-F	Asp43	Halogen (F)	2.82
		C=O	Thr176	H bond	3.29
18	−8.1	C=O	Thr176	H bond	3.02
		-F	Thr202	H bond	2.94
		-F	Gln64	H bond	3.22
		-F	Thr202	H bond	3.55
		-F	Tyr157	Halogen (F)	3.64
		-F	Glu155	Halogen (F)	2.78
		-F	Tyr97	H bond	3.17

(*continued on next page*)

Table 3 (*continued*)

Compounds	Binding Affinity (kcal/mol)	Protein-ligand interactions			
		1 Ligand	Receptors	Interactions	Bonding distance (Å)
		-F	Glu155	Halogen (F)	3.46
		-F	Tyr97	H bond	3.27
VPA	−5.4	-*O*-H	Thr202	H bond	2.55

crystallized BEN500 was isolated from the 4COF and re-docked to the $GABA_A$ receptor (Fig. 3) to record the root mean square deviation (RMSD) of 1.859 Å, and the RMSD <2.0 Å was considered valid. Therefore, the lattice box was accepted and could be used for docking other molecules [50].

In accordance with Table 3, all designed chalcones (**1**–**18**) had binding affinity values between −6.6 and −8.4 kcal/mol, which were higher than the standard drug VPA (−5.4 kcal/mol) and the co-crystallized BEN500 (−6.7 kcal/mol). The binding affinity and selected binding interactions for all the newly designed compounds are also listed in Table 3.

Previously, GABA mimics were prepared chemically using 2,6-difluorophenol (pKa 7.12) and phenol (pKa 9.81) and were used and compared as substrates for the GABA aminotransferase (GABA-AT) assay [51]. Both proved to be GABA-AT competitors but are poor substrates. This suggests that the 2,6-difluorophenol may act as lipophilic bioisosters by mimicking the functionality of the carboxylic acid, similar to phenol. The increased lipophilicity of this moiety should allow new AEDs to better penetrate the BBB. Following this finding, we examined the binding affinity values of the difluoro-containing compounds and found that compound **8** had the highest value (−8.0 kcal/mol) of all the disubstituted chalcones. Although researchers usually correlate experimental IC_{50} values with binding affinity, in most cases it is impossible to obtain a 1:1 correlation between them, which was found in several comprehensive analyses. Therefore, we selected compound **8** as the compound of interest over the most predicted active compound **16** (binding affinity of −8.4 kcal/mol) to study biologically in the in vivo epileptic zebrafish model.

Based on the molecular docking results, several atoms in compound **8** contribute to the strong binding with $GABA_A$ receptor (Fig. 4 and Table 4). The N atom of the pyrrolyl moiety interacted by forming a hydrogen bond with Asn41 within the $GABA_A$ active site. The corresponding heterocyclic pyrrole moiety was also interacted by forming a hydrogen bond with Thr176. It is worth noting that the fluorine atom formed halogen bond with Glu155, in exhibiting its antiepileptic potential. To summarize, the presence of hydrophilic hydrogen and halogen bonds in all the compounds is more important than the hydrophobic π-π-stack and π-σ bonds, highlighting the importance of fluorine substructure in these potential AED candidates. All the 2D and 3D docking illustrations were compiled in Supplementary Material.

3.2. Chemistry

3.2.1. Synthesis

To further validate the in-silico results, (*E*)-3-(3,5-difluorophenyl)-1-(1*H*-pyrrol-2-yl)prop-2-en-1-one (compound **8**) was selected for synthesis. Compound **8** was chemically prepared by a one-pot base-catalyzed Claisen-Schmidt condensation reaction [21] and structurally characterized using X-ray crystallography technique.

3.2.2. X-ray crystallography of (E)-3-(3,5-difluorophenyl)-1-(1h-pyrrol-2-yl)prop-2-en-1-one

Crystals of the predicted active compound **8** were grown by slow evaporation of ethanol, forming 'plate-like' crystals, and the structure was subsequently confirmed by XRD analysis. The asymmetric unit comprises a whole molecule with a structure crystallizing in space group P-1 with Z = 2. The molecular structure is shown in Fig. 5, while the covalent bond lengths and angles are listed in

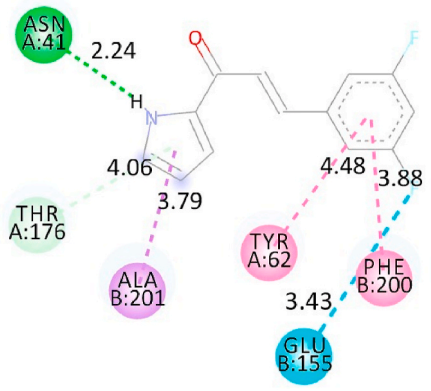

Fig. 4. 2D diagram of the binding interactions of compound **8** with the active site residues of the $GABA_A$ receptor (Green: Hydrogen bonding, Cyan: Halogen (F), pink: π-π stacked, purple: π-σ)

Table 4
Binding affinity and intermolecular interactions of compound **8** against $GABA_A$ enzyme.

Active site	Interactions	With	Distance (Å)
Asn41	Conventional Hydrogen bond	NH	2.24
Tyr62	π-π stacked	Benzene	4.48
Phe200	π-π stacked	Benzene	3.88
Glu155	Halogen (fluorine)	5-F	3.43
Thr176	π-donor Hydrogen Bond	Pyrrole	4.06
Ala201	π-σ	Pyrrole	3.79

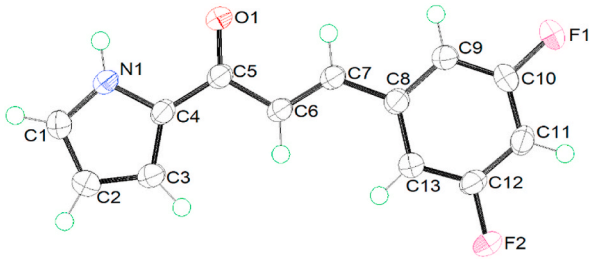

Fig. 5. Molecular structure of compound **8** showing the atom-labelling schemes and displacement ellipsoids at the 70% probability level.

Table 5
Geometric (Å, °) parameter for compound **8**.

Parameter		Parameter		Parameter		Parameter	
F1–C10	1.3547 (13)	C1–N1–C4	109.61 (10)	C5–C6	1.4799 (16)	C9–C8–C7	117.51 (10)
F2–C12	1.3580 (13)	N1–C1–C2	108.53 (11)	C6–C7	1.3349 (17)	C9–C8–C13	119.26 (11)
O1–O5	1.2396 (14)	C1–C2–C3	107.21 (11)	C7–C8	1.4641 (16)	C13–C8–C7	123.22 (11)
N1–C1	1.3495 (16)	C4–C3–C2	107.37 (11)	C8–C9	1.3978 (16)	C10–C9–C8	119.35 (11)
N1–C4	1.3716 (15)	N1–C4–C3	107.28 (10)	C8–C13	1.4020 (16)	F1–C10–C9	118.31 (11)
C1–C2	1.3825 (18)	N1–C4–C5	119.98 (10)	C9–C10	1.3773 (17)	F1–C10–C11	118.56 (11)
C2–C3	1.3989 (17)	C3–C4–C5	132.73 (11)	C10–C11	1.3790 (17)	C9–C10–C11	123.12 (11)
C3–C4	1.3927 (16)	O1–C5–C4	121.00 (11)	C11–C12	1.3818 (17)	C10–C11–C12	115.93 (11)
C4–C5	1.4442 (16)	O1–C5–C6	120.53 (11)	C12–C13	1.3774 (17)	F2–C12–C11	117.38 (10)
		C4–C5–C6	118.46 (10)			F2–C12–C13	118.55 (11)
		C7–C6–C5	119.01 (10)			C13–C12–C11	124.06 (11)
		C6–C7–C8	128.06 (11)			C12–C13–C8	118.26 (11)

Table 5, as well as the crystallographic data and refinement details of compound **8** are summarized in Table S1 (in Supplementary Material). The observed dihedral angles between the centra plane (O1, C5–C7) and the planes of pyrrole (N1, C1–C4) and phenyl (C8–C13) are 6.122° (46) and 0.377° (47), respectively. This means that the molecule has approximately a coplanar conformation. Following the results, the crystal structure of **8** derived from XRD analysis confirms the expected molecular structure as suggested by previous NMR, MS, and FTIR analyses [14]. The discussion of the intermolecular interactions in compound 8 to form a centrosymmetric dimer was detailed in Section S3.2 (in Supplementary Material).

3.3. In vivo studies

3.3.1. Toxicity profiling in zebrafish embryos

Zebrafish is a model animal for neurological studies that has attracted increasing scientific interest over the past two decades. There is ample evidence that zebrafish and mammalian brains share similar neuroanatomical [52] and central neural signalling systems [53] that are relevant to human brain disease. This factor allows for the assessment of the social behavioural disturbances seen in epileptic individuals, in addition to its usefulness in pharmacological studies and/or toxicological research, making the zebrafish a perfect new innovative screening method for drug discovery success and productivity. Prior to determining the optimal safe dosage for compound **8** to be used later in the epilepsy behavioural assay, it was first necessary to establish a toxicity profile of compound **8** for several endpoints, including mortality, tail coiling, and hatching rate.

Assessment of mortality in the zebrafish embryo was essential to determine what concentration of compound **8** at 72 hpf (hours post-fertilization) could have lethal effects on the zebrafish. Mortality could be represented by dead embryos that exhibited mainly coagulation and no heartbeat. Fig. 6A shows the cumulative mortality (%) in zebrafish larvae until hatching (24–72 hpf), where exposure of 12.86 μM or more caused a significant >80% mortality rate, with 21.44 μM already considered lethal at the beginning of the observation period (24 hpf). In contrast, exposure up to 8.58 μM showed no significant difference in mortality compared to the

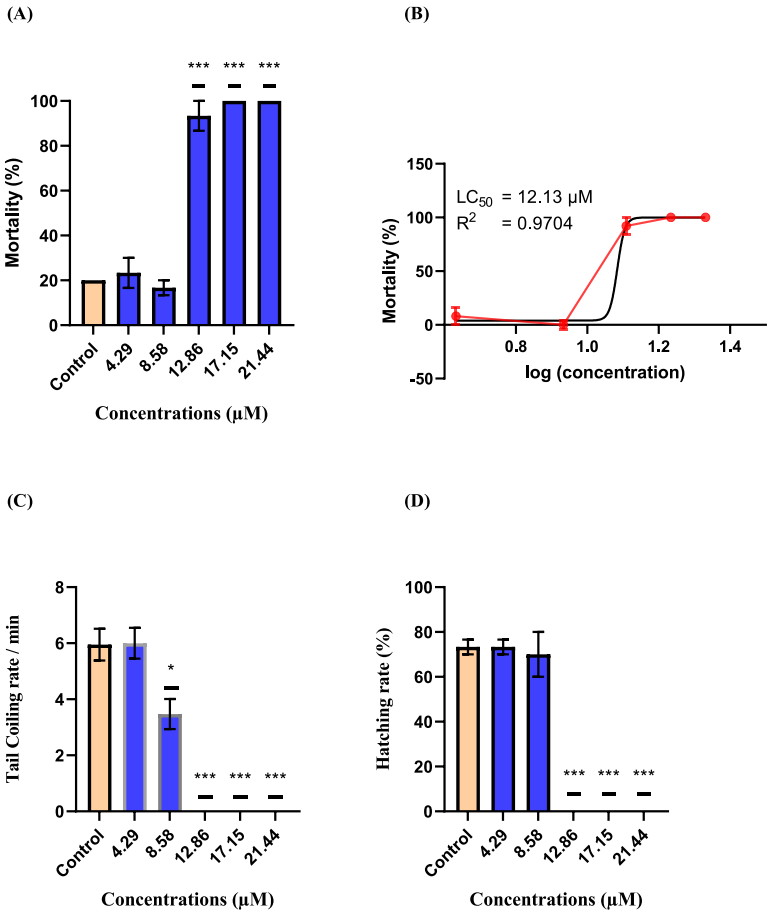

Fig. 6. Toxicity profiles of zebrafish embryos at 24 to 72 hpf based on (**A**) mortality rate, (**B**) LC_{50}, (**C**) spontaneous tail coiling (STC), and (**D**) hatching rate. Results are expressed as mean ± standard error of the mean (SEM) ($n = 30$). Statistical analysis was performed using the one-way analysis of variance (ANOVA) test and a Tukey post-test. (*p < 0.05, **p < 0.01, ***p < 0.001; the p-value is the marginal significance level within a statistical hypothesis test that indicates the probability of a particular event occurring.).

control group. Subsequently, the lethal concentration (LC_{50}) of compound **8**, which killed half of the embryos up to 72 hpf, was calculated to be 12.13 μM (Fig. 6B). Moreover, no significant signs of toxicity were observed in the larval groups exposed to compound **8** up to a concentration of 12.86 μM throughout the exposure period.

Recent studies have shown that the spontaneous tail coiling (STC) movement of zebrafish embryos is an essential indicator to assess the effects of exposed chemicals at the whole organism level, particularly on nervous system development starting at 17 hpf and ending at 28 hpf before more extensive swimming behaviour occurs [54]. This simple movement pattern in zebrafish derives from a basic neural circuit in the spinal cord nervous system and can be altered by structurally diverse neurotoxic compounds. Fig. 6C shows that compound **8** exhibits a significant decrease in STC from 8.58 μM compared to control and no tail movement at 24 hpf after treatment with >12.86 μM, which may indicate that high concentrations of compound **8** disrupt embryonic motor movements [48]. Moreover, the hatching rate in compound **8** treated embryos decreased significantly over time from 12.86 μM (Fig. 6D), indicating that only low dosage does not cause toxic effects in zebrafish embryos as reported in Ref. [55].

In conclusion, based on the profile of all toxicological parameters, the concentration of 8.58 μM was selected as a safe dosage and will be used in the following determination of the antiepileptic effect on the chemically induced zebrafish epilepsy behavioural model.

3.3.2. Antiepileptic effect on PTZ-induced zebrafish epilepsy model

To further validate the antiepileptic effect of the predicted active compound **8**, the fish was first treated with a known chemo-convulsant, pentylenetetrazol (PTZ). Subsequently, various parameters of locomotion were assessed and observed, as motor activity is an ideal behavioural tool for understanding neuronal function. It represents the peak of neuronal integration and is often used to evaluate the neurotoxic effects of compounds [56]. When zebrafish are exposed to PTZ, they exhibit various phases of seizures such as an increase in swimming activity, rapid, whirling, circling swimming behaviour, and brief clonus-like seizures leading to loss of body posture [57]. In addition, the zebrafish PTZ-induced larval model was selected because it is the most ideal in vivo model for screening and identifying small molecule and natural compounds with potential anticonvulsant activity [58,59]. Therefore, the antiepileptic

effect of compound **8** can be assessed by the ability of zebrafish to exhibit normal spontaneous locomotor behaviours, including total and average distance travelled, total and average speed travelled and freezing behaviour (Figs. 7 and 8). Before the actual behavioural test with compound **8** was conducted, the optimal dosage for PTZ (2.5 mM) and VPA (100 μM; positive control) was first adapted based on [30], optimized and used in the following experiment, considering that the dosage used has no lethal effects on zebrafish.

After 1 h of exposure to the tested compounds, the results of zebrafish locomotion (Fig. 6) revealed a significant change in total distance [$F(5, 79) = 15.92$], average distance [$F(5, 76) = 14.50$], total speed [$F(5, 74) = 11.07$], average speed [$F(5, 74) = 15.35$], and distance spent in the inner area [$F(5, 82) = 7.054$] by one-way ANOVA analyses. Comparison between the control and the PTZ group; and between the PTZ and the treatment groups (Tukey test) showed that the application of PTZ significantly increased the distance and speed of zebrafish (Fig. 7A–D). In contrast, the VPA-exposed and compound **8**-treated groups showed a significant decrease in distance (Fig. 7A–B), total velocity (Fig. 7C), and average velocity (Fig. 7D). It is also noteworthy that both compound **8** and VPA treatment significantly increased the distance spent in the inner area (Fig. 7E). These results are consistent with previous studies in which PTZ administration increased locomotion, triggering the epileptic state [60]. Meanwhile, VPA as an AED has been shown to improve the epileptic state due to its ability to inhibit the process of seizure initiation in the CNS [61], with treatment with VPA showing a significant reduction in locomotion of zebrafish larvae [62]. On the other hand, thigmotaxis (or wall hugging) is another parameter for assessing the likelihood of our zebrafish larvae staying close to the edges of an environment [47], and could be an indicator of anxiety behaviour [63,64]. From the results in Fig. 7E, it can be concluded that treatment with compound **8** increases the distance spent in the inner area, suggesting that compound **8** might have anxiolytic properties. This can be further supported by the study in which diazepam, a fast-acting potent anxiolytic, significantly increased the percentage of distance spent in the inner area [65].

In addition to evaluating locomotion in larval zebrafish, freezing behaviour was also quantified using the average number of freezing count and average freezing duration to reveal symptoms of passive larval locomotion, as this may be associated with rigidity in epileptic patients. Freezing is also triggered by avoidance of a new area [65]. Therefore, to detect epileptic behaviour, a correlation

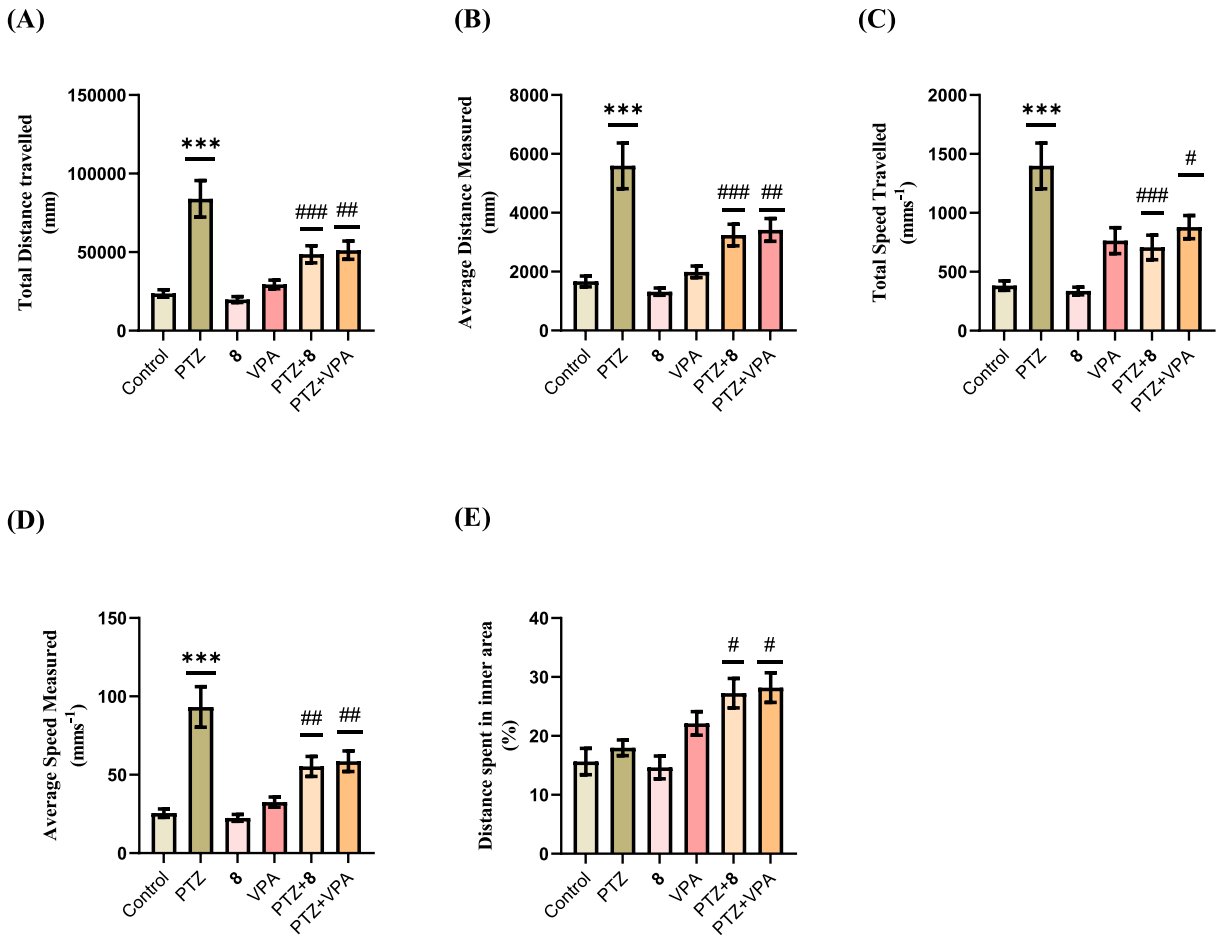

Fig. 7. Locomotor activity in PTZ-induced larvae of zebrafish exposed to the tested compounds at 5 dpf (days post-fertilization). (**A**) Total distance travelled, (**B**) average distance travelled, (**C**) total speed travelled, (**D**) average speed travelled, and (**E**) distance spent in the inner area. Results are presented as mean ± SEM (n = 30). Statistical analysis was performed using one-way ANOVA test followed by Tukey post-test; compared to control (*$p < 0.05$, **$p < 0.01$, ***$p < 0.001$) and compared to PTZ ($^{\#}p < 0.05$, $^{\#\#}p < 0.01$, $^{\#\#\#}p < 0.001$).

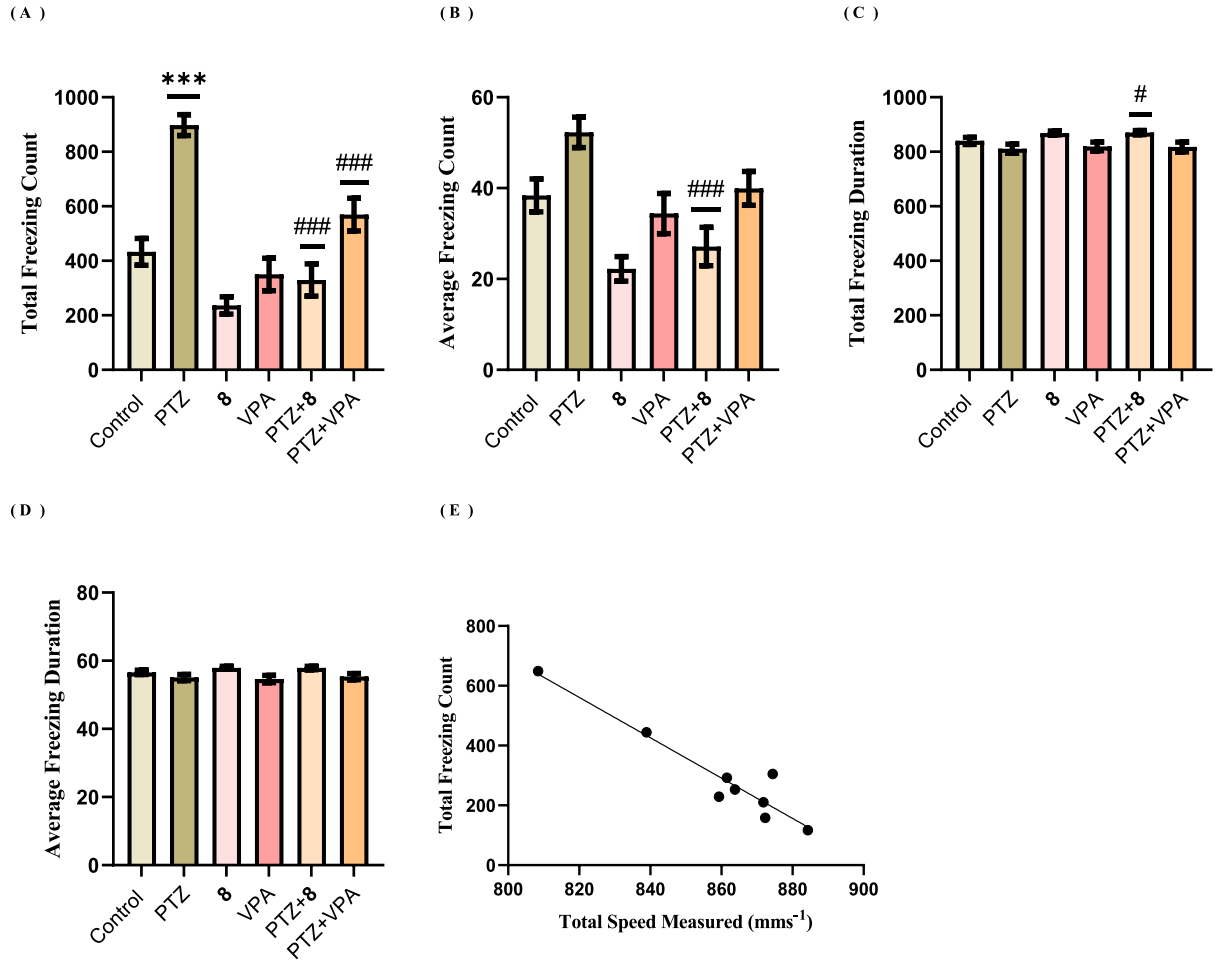

Fig. 8. Quantification of freezing behaviour in PTZ-induced larvae of zebrafish exposed to the tested compounds at 5 dpf. (A) Total freezing count, (B) average freezing count, (C) total freezing duration, (D) average freezing duration, and (E) correlation of total freezing count and total speed measured for the PTZ+**8** group. Results are expressed as mean ± SEM (n = 30). Statistical analysis was performed using a one-way ANOVA test followed by Tukey post-test; compared to control (*p < 0.05, **p < 0.01, ***p < 0.001) and compared to PTZ ($^{\#}$p < 0.05, $^{\#\#}$p < 0.01, $^{\#\#\#}$p < 0.001).

should be made between freezing count and locomotion (in this case, speed). The test was then performed following the PTZ-induced larval zebrafish locomotion procedures, and the results of the freezing behaviour after 1 h of exposure to the tested compounds are shown in Fig. 7.

One-way ANOVA analyses showed a significant difference in the total number of freezes [F (5, 70) = 22.43], the average number of freezing counts [F (5, 83) = 7.782], the total duration of freezes [F (5, 121) = 3.421], and the average duration of freezing count [F (5, 74) = 15.35] of the epileptic zebrafish group treated with compound **8**. The comparison between the control and PTZ groups and between the PTZ and treatment groups (Tukey test) showed that the application of PTZ significantly increased the total number of freezes (Fig. 8A). On the other hand, the compound **8**-treated group showed a significant reduction in the number of freezing count (Fig. 8A–B), while the total duration of freezing episodes increased (Fig. 8C). Similarly, treatment with VPA significantly reduced the total number of freezing count (Fig. 8A) without significant changes in the total duration of freezing count. It is noteworthy that the reduced number of freezing episodes means that epilepsy symptoms such as ictal twitching were reduced. This finding is consistent with the results of [61] that when AEDs such as VPA were used, the number of ictal twitches decreased, suggesting that larvae exhibited fewer jerky movements.

On top of that, there was a significant correlation ($R^2 = 0.91$, $p < 0.001$) between the total number of freezes and the total speed measured in the PTZ-induced group treated with compound **8** (PTZ+**8**; Fig. 8E), indicating the antiepileptic potential of compound **8** to restore zebrafish larvae to a normal state after an epilepsy-induced condition. Overall, in this preliminary study, our compound **8** has been shown to improve locomotion, thigmotaxis, and freezing. Therefore, it could be suggested that it has potential AED properties and warrants in-depth pharmacological studies to develop it as an AED in the near future.

3.3.3. Antiepileptic effect on zc4h2 KO zebrafish epilepsy model

In addition to the PTZ-induced zebrafish epilepsy model, we also tested the effect of compound **8** on a genetically stable knockout (KO) zebrafish epilepsy model to further confirm the antiepileptic efficacy of **8**. We have previously identified mutations of the C4H2-type of zinc finger (ZC4H2) as the causative gene for the rare intellectual disability and developmental disorder (IDD) of Miles-Carpenter syndrome/Wieacker-Wolff syndrome. Miles-Carpenter syndrome is an X-chromosome linked intellectual disability syndrome (XLID, OMIM #312840) [28] and is characterized by microcephaly, spasticity, contractures and epilepsy. Until recently, Miles-Carpenter syndrome was officially renamed 'ZC4H2-associated rare disorder' (ZARD) because it has other clinical features besides intellectual disability.

The human *ZC4H2* gene with five exons is located on the long arm of the X chromosome (Xq11.2) and encodes a protein belonging to the zinc finger domain family. It has been reported that its *C*-terminus consists of a conventional zinc finger domain with four cysteine residues and two histidine residues [66]. *Zc4h2* has an important function in zebrafish nervous system development, as indicated by the fact that its expression is highest during embryonic development and in immature neurons and decreases postnatal and in adult neurons. It is worth noting that *zc4h2* is classified as a potential candidate for X-linked cognitive disability, in which point mutations, rearrangements, and small deletions, could lead to extensive neurodevelopmental impairment of the central and peripheral nervous systems [67].

When we mimic the disease, larvae of the homozygous *zc4h2* KO mutant zebrafish model exhibit abnormal swimming, increased twitching, motor hyperactivity, deficits in eye movement, and pectoral fin contractures [28,68], reminiscent of human patients with a *ZC4H2* mutation. The results suggest that the zebrafish model *zc4h2* KO model could be used to investigate the underlying cellular mechanisms of interneuronopathy and movement disorders, including epilepsy [28]. To further support the justification of the selected mutant model, we previously performed a phenotype-based screen of 6.566 small molecules using this zebrafish model *zc4h2* KO model to identify 4-(2-chloro-4-fluorobenzyl)-3-(2-thienyl)-1,2,4-oxadiazol-5(4*H*)-one (GM90432), a novel antiseizure molecule that effectively cross the blood-brain barrier and distribute in the brain [69].

In this study, we used the ZEBRA device to phenotypically test compound **8** in the zebrafish KO epilepsy model. This particular device is a microfluidic restriction array designed to immobilize zebrafish larvae for rapid and convenient recording over time while allowing the administration of chemicals/reagents directly into the capillary tube via access ports (as shown in Fig. 9) [70]. The restriction assay was used to detect hyperactivity in *zc4h2* KO zebrafish larvae at 5 dpf. This allowed a detailed comparison of phenotype between treated KO, untreated KO, and untreated wild-type (WT) sibling zebrafish ($n = 6$ larvae) placed in a separate ZEBRA device.

We treated *zc4h2* KO zebrafish larvae with different concentrations of compound **8** (2.5, 5, 10, 20, 40 and 80 μM) together with a positive (KO control 0.1% DMSO) and a negative control (WT sibling) in 48 well plates ($n = 6$ per well). To determine if this hyperactivity could be inhibited by compound **8**, *zc4h2* KO larvae exposed to compound **8** were subjected to partial epilepsy treatment for 2 h. The movement patterns of each larva were recorded with the ZEBRA device on the Leica DFC450C digital camera (Leica TL5000 Ergo transmitted-light base) and processed with the Leica Application Suite (Leica, Wetzlar, Germany). The number of jaw movements per minute were then counted for each zebrafish larva for observation. As can be seen in Fig. 10A, larvae treated with compound **8** show reduced jaw movements than the control groups up to a concentration of 10 μM. This concentration is within the range of optimal safe and LC_{50} concentrations of 8.58 μM and 12.13 μM found in the PTZ-induced epileptic zebrafish model, indicating the potential of compound **8** as a new alternative AED agent.

In addition, heart beating rate was also examined, as fluctuations in heart rhythm can lead to cardiac system dysfunction in zebrafish [71]. Therefore, to test whether compound **8** could cause cardiotoxicity we measured the heartbeat of each larva by treating larvae with different concentrations of compound **8** ($n = 10$ larvae) per well in a 48-well plate and incubating them for 2 h. After incubation, heartbeats/min were counted using a Leica DFC450C digital camera (Leica TL5000 Ergo transmitted light base). Fig. 10B shows that there is no significant difference between the heartbeats of the **8**-treated larvae and those of the control groups. This shows that compound **8** has no potential cardiotoxicity, indicating its non-harmful property, and that it is considered safe to consume.

4. Conclusion

This study could serve as preliminary results for the discovery and development of a new antiepileptic drug candidate from a series of fluorine-containing pyrrolylated chalcones. The search began with the design of compounds, which were then subjected to in silico filtering. This revealed that all eighteen newly designed compounds (**1**–**18**) showed good drug-likeness characteristics. Molecular docking was then performed to clarify the binding affinity and chemical interaction between the designed chalcones (**1**–**18**) and the $GABA_A$ receptor. Among all, (*E*)-1-(1*H*-pyrrol-2-yl)-3-(3,5-difluorophenyl)prop-2-en-1-one (compound **8**) showed significant binding affinity with −8.0 kcal/mol, higher than the standard AED, VPA (−5.4 kcal/mol), with predicted good BBB property. Consequently, compound **8** was synthesized and structurally characterized by single crystal X-ray diffraction method. Moreover, exposure of compound **8** (LC_{50} of 8.58 μM) to PTZ-induced epilepsy in zebrafish larvae resulted in a significant reduction in the number of distances travelled and freezing count, which is comparable to the effect of standard AED, VPA. This antiepileptic potential was further verified in a genetic epilepsy model of *zc4h2* KO zebrafish, which showed a reduction in hyperactive jaw movements up to 10 μM. In addition, no cardiotoxic effects was observed, indicating a non-harmful property of **8**. The overall results suggest that pyrrolylated chalcones could serve as a new template for AEDs and warrant an in-depth pharmacological efficacy study to uncover their mechanism of action. Although zebrafish are more advantageous, i.e., easy to handle, low cost and produce rapid throughput, and can be used in the pre-regulatory phase of drug development. However, further validation studies with mammalian rodents in vivo, ex vivo and clinical trials are essential to overcome industry scepticism. It is also worth mentioning that zebrafish does not challenge the position of rodent

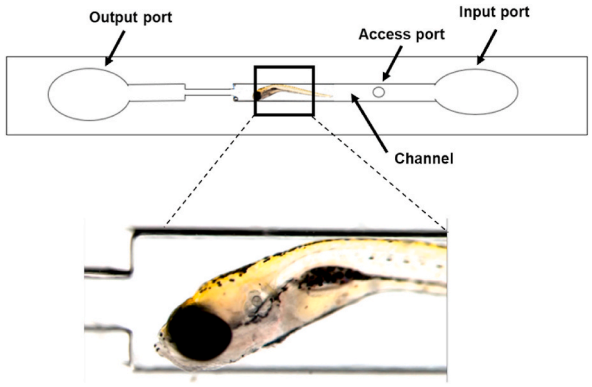

Fig. 9. ZEBRA device for phenotypic study of compound **8** using the *zc4h2* zebrafish KO epilepsy in vivo model.

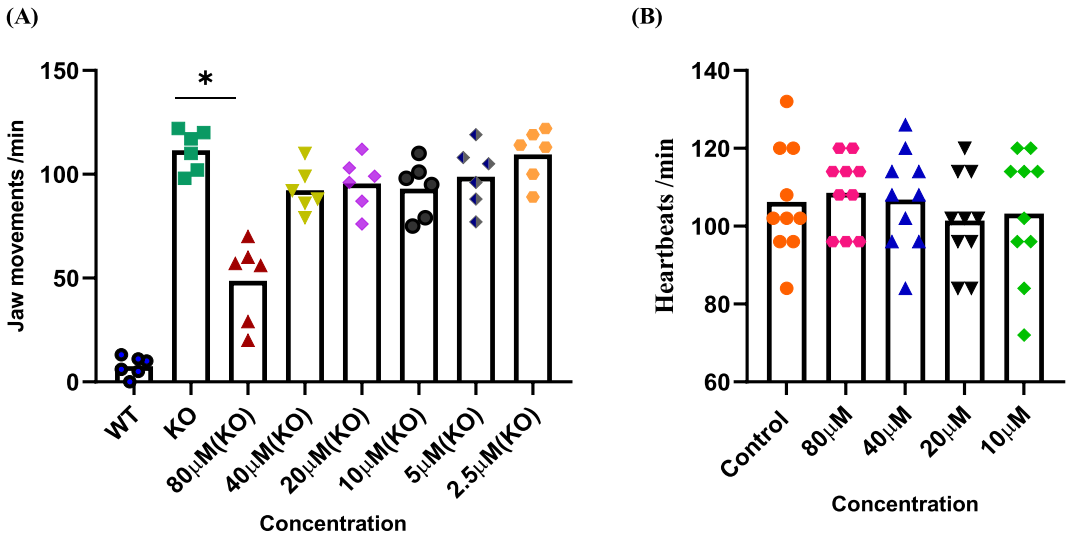

Fig. 10. (**A**) Jaw movements and (**B**) heartbeat of 5 dpf larvae of zebrafish *zc4h2* KO epilepsy after exposure to compound **8**.

models, but rather complements them, especially in the early stages of drug discovery, thus validating their use as alternative animal models.

Author contribution statement

Muhammad Syafiq Akmal Mohd Fahmi, Puspanjali Swain: Performed the experiments; Analyzed and interpreted the data; Wrote the paper.

Amirah Hani Ramli, Nur Atikah Saleh Hodin, Noraini Abu Bakar: Analyzed and interpreted the data.

Wan Norhamidah Wan Ibrahim, Yee Seng Tan, Siti Munirah Mohd Faudzi: Conceived and designed the experiments; Analyzed and interpreted the data; Contributed reagents, materials, analysis tools or data; Wrote the Paper.

Cheol-Hee Kim: Conceived and designed the experiments; Analyzed and interpreted the data; Contributed reagents, materials, analysis tools or data.

Funding statement

Dr. Siti Munirah Mohd Faudzi was supported by Ministry of Higher Education, Malaysia [FRGS/1/2018/STG01/UPM/02/8]. Cheol-Hee Kim was supported by National Research Foundation of Korea [2020R1A5A8017671 & 2021R1A2C1008506].

Data availability statement

Data associated with this study has been deposited at the Cambridge Crystallographic Data Center (CCDC) under the accession

number (Deposit Number: 2,203,560).

Declaration of interest's statement

The authors declare no conflict of interest.

Appendix A. Supplementary data

Supplementary data to this article can be found online at https://doi.org/10.1016/j.heliyon.2023.e13685.

References

[1] T. Musumeci, A. Bonaccorso, G. Puglisi, Epilepsy disease and nose-to-brain delivery of polymeric nanoparticles: an overview, Pharmaceutics 11 (3) (2019), https://doi.org/10.3390/pharmaceutics11030118.

[2] S.-L. Fong, K.-S. Lim, L. Tan, N.H. Zainuddin, J.-H. Ho, Z.-J. Chia, W.-Y. Choo, S.D. Puvanarajah, S. Chinnasami, S.-K. Tee, A.A. Raymond, W.-C. Law, C.-T. Tan, Prevalence study of epilepsy in Malaysia, Epilepsy Res. 170 (2021), 106551, https://doi.org/10.1016/j.eplepsyres.2021.106551.

[3] R.S. Fisher, W.v.E. Boas, W. Blume, C. Elger, P. Genton, P. Lee, J. Engel Jr., Epileptic seizures and epilepsy: definitions proposed by the international league against epilepsy (ILAE) and the international bureau for epilepsy (IBE), Epilepsia 46 (4) (2005) 470–472, https://doi.org/10.1111/j.0013-9580.2005.66104.x.

[4] O.C. González, G.P. Krishnan, I. Timofeev, Ionic and synaptic mechanisms of seizure generation and epileptogenesis, Neurobiol. Dis. 130 (2019), 104485, https://doi.org/10.1016/j.nbd.2019.104485.

[5] G.L. Sarlo, K.F. Holton, Brain concentrations of glutamate and GABA in human epilepsy: a review, Seizure 91 (2021) 213–227, https://doi.org/10.1016/j.seizure.2021.06.028.

[6] W.C. Chen, E.Y. Chen, R.Z. Gebre, M.R. Johnson, N. Li, P. Vitkovskiy, Epilepsy and driving: potential impact of transient impaired consciousness, Epilepsy Behav. 30 (2014) 50–57, https://doi.org/10.1016/j.yebeh.2013.09.024.

[7] B.W. Abou-Khalil, Update on antiepileptic drugs 2019, CONTIN. Lifelong learn, Neurol. 25 (2) (2019), https://doi.org/10.1212/CON.0000000000000715.

[8] S. Uzun, O. Kozumplik, M. Jakovljević, B. Sedić, Side effects of treatment with benzodiazepines, Psychiatr. Danub. 22 (1) (2010) 90–93. PMID: 20305598.

[9] V. Yerragunta, T. Kumaraswamy, D. Suman, V. Anusha, P. Patil, A review on Chalcones and its importance, Pharma 1 (2013) 54–59. https://www.pharmatutor.org/articles/review-on-chalcones-its-importance. (Accessed 20 November 2013). accessed.

[10] W. Dan, J. Dai, Recent developments of chalcones as potential antibacterial agents in medicinal chemistry, Eur. J. Med. Chem. 187 (2020), 111980, https://doi.org/10.1016/j.ejmech.2019.111980.

[11] B.K.M. Choo, U.P. Kundap, S.M. Mohd Faudzi, F. Abas, M.F. Shaikh, É. Samarut, Identification of curcumin analogues with anti-seizure potential in vivo using chemical and genetic zebrafish larva seizure models, Biomed. Pharmacother. 142 (2021), 112035, https://doi.org/10.1016/j.biopha.2021.112035.

[12] R.S. Cheke, S.D. Shinde, J.P. Ambhore, S.R. Chaudhari, S.B. Bari, Quinazoline, An update on current status against convulsions, J. Mol. Struct. 1248 (2022), 131384, https://doi.org/10.1016/j.molstruc.2021.131384.

[13] S.M. Hashemi, S. Emami, P. Honarchian Masihi, A. Shakiba, L. Dehestani, N. Ahangar, Synthesis of 2-aryl-3-triazolyl-indoles from phenacyltriazole-derived hydrazones: exploring new scaffolds for anticonvulsant activity, J. Mol. Struct. 1276 (2023), 134704, https://doi.org/10.1016/j.molstruc.2022.134704.

[14] V.R. Solomon, V.J. Tallapragada, M. Chebib, G.A.R. Johnston, J.R. Hanrahan, GABA allosteric modulators: an overview of recent developments in non-benzodiazepine modulators, Eur. J. Med. Chem. 171 (2019) 434–461, https://doi.org/10.1016/j.ejmech.2019.03.043.

[15] V. Natchimuthu, S. Bandaru, A. Nayarisseri, S. Ravi, Design, synthesis and computational evaluation of a novel intermediate salt of N-cyclohexyl-N-(cyclohexylcarbamoyl)-4-(trifluoromethyl) benzamide as potential potassium channel blocker in epileptic paroxysmal seizures, Comput. Biol. Chem. 64 (2016) 64–73, https://doi.org/10.1016/j.compbiolchem.2016.05.003.

[16] A. Ayati, S. Emami, A. Foroumadi, The importance of triazole scaffold in the development of anticonvulsant agents, Eur. J. Med. Chem. 109 (2016) 380–392, https://doi.org/10.1016/j.ejmech.2016.01.009.

[17] V. Karthick, T.P.P. Selvam, P.V. Kumar, P. Ramu, Antiepileptic properties of novel 2-(substituted benzylidene)-7-(4-chlorophenyl)-5-(furan-2-yl)-2 H -thiazolo [3,2 -a]pyrimidin-3(7 H)-one derivatives, J. Saudi Chem. Soc. 20 (2016) S1–S6, https://doi.org/10.1016/j.jscs.2012.07.018.

[18] A. Satoh, Y. Nagatomi, Y. Hirata, S. Ito, G. Suzuki, T. Kimura, S. Maehara, H. Hikichi, A. Satow, M. Hata, H. Ohta, H. Kawamoto, Discovery and in vitro and in vivo profiles of 4-fluoro-N-[4-[6-(isopropylamino)pyrimidin-4-yl]-1,3-thiazol-2-yl]-N-methylbenzamide as novel class of an orally active metabotropic glutamate receptor 1 (mGluR1) antagonist, Bioorg. Med. Chem. Lett. 19 (18) (2009) 5464–5468, https://doi.org/10.1016/j.bmcl.2009.07.097.

[19] P. Shah, A.D. Westwell, The role of fluorine in medicinal chemistry, J. Enzym. Inhib. Med. Chem. 22 (5) (2007) 527–540, https://doi.org/10.1080/14756360701425014.

[20] T.-Y. Choi, T.-I. Choi, Y.-R. Lee, S.-K. Choe, C.-H. Kim, Zebrafish as an animal model for biomedical research, Exp. Mol. Med. 53 (3) (2021) 310–317, https://doi.org/10.1038/s12276-021-00571-5.

[21] M. Gunasekharan, T.-I. Choi, Y. Rukayadi, M.A. Mohammad Latif, T. Karunakaran, S.M. Mohd Faudzi, C.-H. Kim, Preliminary insight of pyrrolylated-chalcones as new anti-methicillin-resistant Staphylococcus aureus (Anti-MRSA) agents, Molecules 26 (17) (2021), https://doi.org/10.3390/molecules26175314.

[22] O. Rigaku, Diffraction, CrysAlis PRO, Yarnton, Oxfordshire, England, 2017 (Version 42).

[23] G.M. Sheldrick, A short history of SHELX, Acta Crystallogr. A. 64 (2008) 112–122, https://doi.org/10.1107/S0108767307043930.

[24] G.M. Sheldrick, Crystal structure refinement with SHELXL, Acta Crystallogr. C Struct. Chem. 71 (2015) 3–8, https://doi.org/10.1107/S2053229614024218.

[25] L.J. Farrugia, WinGX and ORTEP for Windows: an update, J. Appl. Crystallogr. 45 (2012) 849–854, https://doi.org/10.1107/S0021889812029111.

[26] A.L. Spek, *checkCIF* validation ALERTS: what they mean and how to respond, Acta Crystallogr. E: Crystallogr. Commun. 76 (2020) 1–11, https://doi.org/10.1107/S2056989019016244.

[27] K. Brandenburg, DIAMOND, Diamond 4.6.8, Crystal Impact GbR, Bonn, Germany, 2006 (Version 4.6.8).

[28] M. May, K.-S. Hwang, J. Miles, C. Williams, T. Niranjan, S.G. Kahler, P. Chiurazzi, K. Steindl, P.J. Van Der Spek, S. Swagemakers, J. Mueller, S. Stefl, E. Alexov, J.-I. Ryu, J.-H. Choi, H.-T. Kim, P. Tarpey, G. Neri, L. Holloway, C. Skinner, R.E. Stevenson, R.I. Dorsky, T. Wang, C.E. Schwartz, C.-H. Kim, ZC4H2, an XLID gene, is required for the generation of a specific subset of CNS interneurons, Hum. Mol. Genet. 24 (17) (2015) 4848–4861, https://doi.org/10.1093/hmg/ddv208.

[29] A.A.S. de Oliveira, T.A.V. Brigante, D.P. Oliveira, Tail coiling assay in zebrafish (Danio rerio) embryos: stage of development, promising positive control candidates, and selection of an appropriate organic solvent for screening of developmental neurotoxicity (DNT), Water 13 (2) (2021), https://doi.org/10.3390/w13020119.

[30] D.A. Feas, D.E. Igartúa, M.N. Calienni, C.S. Martinez, M. Pifano, N.S. Chiaramoni, S. del Valle Alonso, M.J. Prieto, Nutraceutical emulsion containing valproic acid (NE-VPA): a drug delivery system for reversion of seizures in zebrafish larvae epilepsy model, J. Pharm. Investig. 47 (5) (2017) 429–437, https://doi.org/10.1007/s40005-017-0316-x.

[31] X. Peng, J. Lin, Y. Zhu, X. Liu, Y. Zhang, Y. Ji, X. Yang, Y. Zhang, N. Guo, Q. Li, Anxiety-related behavioral responses of pentylenetetrazole-treated zebrafish larvae to light-dark transitions, Pharmacol. Biochem. Behav. 145 (2016) 55–65, https://doi.org/10.1016/j.pbb.2016.03.010.

[32] N. Abu Bakar, W.N. Wan Ibrahim, C.A. Che Abdullah, N.F. Ramlan, K. Shaari, S. Shohaimi, A. Mediani, N.S. Nasruddin, C.-H. Kim, S.M. Mohd Faudzi, Embryonic arsenic exposure triggers long-term behavioral impairment with metabolite alterations in zebrafish, Toxics 10 (9) (2022) 493, https://doi.org/10.3390/toxics10090493.

[33] S. Brogi, T.C. Ramalho, K. Kuca, J.L. Medina-Franco, M. Valko, Editorial: *In silico* methods for drug design and discovery, Front. Chem. 8 (2020) 612, https://doi.org/10.3389/fchem.2020.00612.

[34] Physicochemical properties and environmental fate, in: A Framework to Guide Selection of Chemical Alternatives, The National Academies Press, Washington, DC, 2014, p. 47, https://doi.org/10.17226/18872.

[35] C.A. Lipinski, F. Lombardo, B.W. Dominy, P.J. Feeney, Experimental and computational approaches to estimate solubility and permeability in drug discovery and development settings, Adv. Drug Deliv. Rev. 23 (1) (1997) 3–25, https://doi.org/10.1016/S0169-409X(96)00423-1.

[36] B.T. Fernandes, C.F.M. Segretti, C.M. Polli, R. Parise-Filho, Analysis of the applicability and use of Lipinski's rule for central nervous system drugs, Lett. Drug Des. Discov. 13 (10) (2016) 999–1006, https://doi.org/10.2174/1570180813666160622092839.

[37] M.A. Abdullah, Y.-R. Lee, S.N. Mastuki, S.W. Leong, W.N. Wan Ibrahim, M.A. Mohammad Latif, A.N.M. Ramli, M.F.F. Mohd Aluwi, S.M. Mohd Faudzi, C.-H. Kim, Development of diarylpentadienone analogues as alpha-glucosidase inhibitor: synthesis, in vitro biological and in vivo toxicity evaluations, and molecular docking analysis, Bioorg. Chem. 104 (2020), 104277, https://doi.org/10.1016/j.bioorg.2020.104277.

[38] J.J. Irwin, D. Duan, H. Torosyan, A.K. Doak, K.T. Ziebart, T. Sterling, G. Tumanian, B.K. Shoichet, An aggregation advisor for ligand discovery, J. Med. Chem. 58 (17) (2015) 7076–7087, https://doi.org/10.1021/acs.jmedchem.5b01105.

[39] D. Craciun, D. Modra, A. Isvoran, ADME-Tox profiles of some food additives and pesticides, AIP Conf. Proc. 1694 (1) (2015), 040007, https://doi.org/10.1063/1.4937259.

[40] A.B. Gurung, A. Bhattacharjee, M.A. Ali, Exploring the physicochemical profile and the binding patterns of selected novel anticancer Himalayan plant derived active compounds with macromolecular targets, Inform. Med. Unlocked 5 (2016) 1–14, https://doi.org/10.1016/j.imu.2016.09.004.

[41] F. Lovering, J. Bikker, C. Humblet, Escape from flatland: increasing saturation as an approach to improving clinical success, J. Med. Chem. 52 (21) (2009) 6752–6756, https://doi.org/10.1021/jm901241e.

[42] W. Wei, S. Cherukupalli, L. Jing, X. Liu, P. Zhan, Fsp3: a new parameter for drug-likeness, Drug Discov 25 (10) (2020) 1839–1845, https://doi.org/10.1016/j.drudis.2020.07.017.

[43] M.P. Doogue, T.M. Polasek, The ABCD of clinical pharmacokinetics, Ther. Adv. Drug Saf. 4 (1) (2013) 5–7, https://doi.org/10.1177/2042098612469335.

[44] A.M.M. Jokipii, V.V. Myllylä, E. Hokkanen, L. Jokipii, Penetration of the blood brain barrier by metronidazole and tinidazole, J. Antimicrob. Chemother. 3 (3) (1977) 239–245, https://doi.org/10.1093/jac/3.3.239.

[45] M.C.F.C.B. Damião, K.F.M. Pasqualoto, M.C. Polli, R. Parise Filho, To Be drug or prodrug: structure-property exploratory approach regarding oral bioavailability, J. Pharm. Pharmaceut. Sci. 17 (4) (2014) 532–540, https://doi.org/10.18433/J3BS4H.

[46] L. Dean, M. Kane, Omeprazole therapy and CYP2C19 genotype, in: V.M. Pratt, S.A. Scott, M. Pirmohamed, B. Esquivel, M.S. Kane, B.L. Kattman, A.J. Malheiro (Eds.), Medical Genetics Summaries, National Center for Biotechnology Information (US), Bethesda (MD), 2012. PMID: 28520353.

[47] T.A. Sonia, C.P. Sharma, Oral Delivery of Insulin, Woodhead Publishing Series in Biomedicine, vol. 1, Woodhead Publishing, 2014, pp. 128–129.

[48] T. Bohnert, L.-S. Gan, Plasma protein binding: from discovery to development, J. Pharmacol. Sci. 102 (9) (2013) 2953–2994, https://doi.org/10.1002/jps.23614.

[49] P.S. Miller, A.R. Aricescu, Crystal structure of a human $GABA_A$ receptor, Nature 512 (7514) (2014) 270–275, https://doi.org/10.1038/nature13293.

[50] C. Granchi, A. Capecchi, G. Del Frate, A. Martinelli, M. Macchia, F. Minutolo, T. Tuccinardi, Development and validation of a docking-based virtual screening platform for the identification of new lactate dehydrogenase inhibitors, Molecules 20 (5) (2015) 8772–8790, https://doi.org/10.3390/molecules20058772.

[51] J. Qiu, S.H. Stevenseon, M.J. O'Beirne, R.B. Silverman, ChemInform abstract: 2,6-difluorophenol as a bioisostere of a carboxylic acid: bioisosteric analogues of γ-aminobutyric acid, ChemInform 30 (23) (1999), https://doi.org/10.1021/jm980435l.

[52] T. Mueller, M.F. Wullimann, An evolutionary interpretation of teleostean forebrain anatomy, Brain Behav. Evol. 74 (1) (2009) 30–42, https://doi.org/10.1159/000229011.

[53] K.A. Horzmann, J.L. Freeman, Zebrafish get connected: investigating neurotransmission targets and alterations in chemical toxicity, Toxics 4 (3) (2016), https://doi.org/10.3390/toxics4030019.

[54] L.D. Knogler, J. Ryan, L. Saint-Amant, P. Drapeau, A hybrid electrical/chemical circuit in the spinal cord generates a transient embryonic motor behavior, J. Neurosci. Res. 34 (29) (2014) 9644, https://doi.org/10.1523/JNEUROSCI.1225-14.2014.

[55] J. Lodovichi, E. Landucci, L. Pitto, I. Gisone, M. D'Ambrosio, C. Luceri, M.C. Salvatici, M.C. Bergonzi, Evaluation of the increase of the thymoquinone permeability formulated in polymeric micelles: in vitro test and in vivo toxicity assessment in Zebrafish embryos, Eur. J. Pharmaceut. Sci. 169 (2022), 106090, https://doi.org/10.1016/j.ejps.2021.106090.

[56] V.C. Moser, Functional assays for neurotoxicity testing, Toxicol. Pathol. 39 (1) (2010) 36–45, https://doi.org/10.1177/0192623310385255c.

[57] P. Gupta, S.B. Khobragade, V.M. Shingatgeri, Effect of various antiepileptic drugs in zebrafish PTZ-seizure model, Indian J. Pharmaceut. Sci. 76 (2) (2014) 157–163. PMID: 24843189.

[58] S. Challal, O.E.M. Buenafe, E.F. Queiroz, S. Maljevic, L. Marcourt, M. Bock, W. Kloeti, F.M. Dayrit, A.L. Harvey, H. Lerche, C.V. Esguerra, P.A.M. de Witte, J.-L. Wolfender, A.D. Crawford, Zebrafish bioassay-guided microfractionation identifies anticonvulsant steroid glycosides from the philippine medicinal plant solanum torvum, ACS Chem. Neurosci. 5 (10) (2014) 993–1004, https://doi.org/10.1021/cn5001342.

[59] A.M. Orellana-Paucar, T. Afrikanova, J. Thomas, Y.K. Aibuldinov, W. Dehaen, P.A.M. de Witte, C.V. Esguerra, Insights from zebrafish and mouse models on the activity and safety of Ar-turmerone as a potential drug candidate for the treatment of epilepsy, PLoS One 8 (12) (2013), e81634, https://doi.org/10.1371/journal.pone.0081634.

[60] B.H.M. Mussulini, C.E. Leite, K.C. Zenki, L. Moro, S. Baggio, E.P. Rico, D.B. Rosemberg, R.D. Dias, T.M. Souza, M.E. Calcagnotto, M.M. Campos, A.M. Battastini, D.L. de Oliveira, Seizures induced by pentylenetetrazole in the adult zebrafish: a detailed behavioral characterization, PLoS One 8 (1) (2013), e54515, https://doi.org/10.1371/journal.pone.0054515.

[61] M. Romoli, P. Mazzocchetti, R. D'Alonzo, S. Siliquini, E.V. Rinaldi, A. Verrotti, P. Calabresi, C. Costa, Valproic acid and epilepsy: from molecular mechanisms to clinical evidences, Curr. Neuropharmacol. 17 (10) (2019) 926–946, https://doi.org/10.2174/1570159X17666181227165722.

[62] P. Shaw, P. Mondal, A. Dey Bhowmik, A. Bandyopadhyay, M. Sudarshan, A. Chakraborty, A. Chattopadhyay, Environmentally relevant hexavalent chromium disrupts elemental homeostasis and induces apoptosis in zebrafish liver, Bull. Environ. Contam. Toxicol. 108 (4) (2022) 716–724, https://doi.org/10.1007/s00128-021-03427-w.

[63] X. Peng, J. Lin, Y. Zhu, X. Liu, Y. Zhang, Y. Ji, X. Yang, Y. Zhang, N. Guo, Q. Li, Anxiety-related behavioral responses of pentylenetetrazole-treated zebrafish larvae to light-dark transitions, Pharmacol. Biochem. Behav. 145 (2016) 55–65, https://doi.org/10.1016/j.pbb.2016.03.010.

[64] S.J. Schnörr, P.J. Steenbergen, M.K. Richardson, D.L. Champagne, Measuring thigmotaxis in larval zebrafish, Behav, Brain Res. 228 (2) (2012) 367–374, https://doi.org/10.1016/j.bbr.2011.12.016.

[65] R.M. Colwill, R. Creton, Locomotor behaviors in zebrafish (Danio rerio) larvae, Behav. Process. 86 (2) (2011) 222–229, https://doi.org/10.1016/j.beproc.2010.12.003.

[66] D. Wang, D. Hu, Z. Guo, R. Hu, Q. Wang, Y. Liu, M. Liu, Z. Meng, H. Yang, Y. Zhang, F. Cai, W. Zhou, W. Song, A novel de novo nonsense mutation in ZC4H2 causes Wieacker-Wolff Syndrome, Mol. Genet. Genomic Med. 8 (2) (2020), e1100, https://doi.org/10.1002/mgg3.1100.

[67] H. Hirata, I. Nanda, A. van Riesen, G. McMichael, H. Hu, M. Hambrock, M.-A. Papon, U. Fischer, S. Marouillat, C. Ding, S. Alirol, M. Bienek, S. Preisler-Adams, A. Grimme, D. Seelow, R. Webster, E. Haan, A. MacLennan, W. Stenzel, Tzu Y. Yap, A. Gardner, Lam S. Nguyen, M. Shaw, N. Lebrun, Stefan A. Haas, W. Kress, T. Haaf, E. Schellenberger, J. Chelly, G. Viot, Lisa G. Shaffer, Jill A. Rosenfeld, N. Kramer, R. Falk, D. El-Khechen, Luis F. Escobar, R. Hennekam, P. Wieacker, C. Hübner, H.-H. Ropers, J. Gecz, M. Schuelke, F. Laumonnier, Vera M. Kalscheuer, ZC4H2 mutations are associated with arthrogryposis multiplex congenita and intellectual disability through impairment of central and peripheral synaptic plasticity, Am. J. Hum. Genet. 92 (5) (2013) 681–695, https://doi.org/10.1016/j.ajhg.2013.03.021.

[68] S.G.M. Frints, F. Hennig, R. Colombo, S. Jacquemont, P. Terhal, H.H. Zimmerman, D. Hunt, B.A. Mendelsohn, U. Kordaß, R. Webster, M. Sinnema, O. Abdul-Rahman, V. Suckow, A. Fernández-Jaén, K. van Roozendaal, S.J.C. Stevens, M.V.E. Macville, S. Al-Nasiry, K. van Gassen, N. Utzig, S.M. Koudijs, L. McGregor, S. M. Maas, D. Baralle, A. Dixit, P. Wieacker, M. Lee, A.S. Lee, E.C. Engle, G. Houge, G.A. Gradek, A.G.L. Douglas, C. Longman, S. Joss, D. Velasco, R.C. Hennekam, H. Hirata, V.M. Kalscheuer, Deleterious de novo variants of X-linked ZC4H2 in females cause a variable phenotype with neurogenic arthrogryposis multiplex congenita, Hum. Mutat. 40 (12) (2019) 2270–2285, https://doi.org/10.1002/humu.23841.

[69] K.-S. Hwang, H. Kan, S.S. Kim, J.S. Chae, J.Y. Yang, D.-S. Shin, S.H. Ahn, J.H. Ahn, J.-H. Cho, I.-S. Jang, J. Shin, J. Joo, C.-H. Kim, M.A. Bae, Efficacy and pharmacokinetics evaluation of 4-(2-chloro-4-fluorobenzyl)-3-(2-thienyl)-1,2,4-oxadiazol-5(4H)-one (GM-90432) as an anti-seizure agent, Neurochem. Int. 141 (2020), 104870, https://doi.org/10.1016/j.neuint.2020.104870.

[70] T.I. Hong, K.-S. Hwang, T.-I. Choi, G. Kleinau, P. Scheerer, J.K. Bang, S.-H. Jung, C.-H. Kim, Zebrafish bioassay for screening therapeutic candidates based on melanotrophic activity, Int. J. Mol. Sci. 22 (17) (2021), https://doi.org/10.3390/ijms22179313.

[71] E. De Luca, G.M. Zaccaria, M. Hadhoud, G. Rizzo, R. Ponzini, U. Morbiducci, M.M. Santoro, ZebraBeat: a flexible platform for the analysis of the cardiac rate in zebrafish embryos, Sci. Rep. 4 (1) (2014) 4898, https://doi.org/10.1038/srep04898.